Research Square

Preprints are preliminary reports that have not undergone peer review.
They should not be considered conclusive, used to inform clinical practice,
or referenced by the media as validated information.

COVID-19 pathophysiology may be driven by a loss of inhibition of the Renin-Angiotensin-Aldosterone System

Susanne Rysz
Karolinska Institutet, Karolinska University Hospital
Jonathan Al-Saadi
Karolinska Institutet
Anna Sjöström
Karolinska Institutet and Karolinska University Hospital
Maria Farm
Karolinska Institutet, Karolinska University Hospital
Francesca Campoccia Jalde
Karolinska University Hospital, Karolinska Institutet
Michael Plattén
Karolinska Institutet and Karolinska University Hospital
Helen Eriksson
Stockholm University
Margareta Klein
Karolinska Institutet, Karolinska University Hospital
Roberto Vargas-Paris
Karolinska Institutet, Karolinska University Hospital
Sven Nyrén
Karolinska Institutet, Karolinska University Hospital
Goran Abdula
Karolinska Institutet, Karolinska University Hospital
Russell Ouellette
Karolinska Institutet, Karolinska University Hospital
Tobias Granberg
Karolinska Institutet, Karolinska University Hospital
Malin Jonsson Fagerlund
Karolinska University Hospital, Karolinska Institutet
Johan Lundberg (✉ j.lundberg@ki.se)
Karolinska Institutet

Research Article

Keywords: COVID-19, SARS-CoV-2, ACEII, Angiotensin, Swine, MRI, MRI-pefusion, CTPA, Echocardiography

Posted Date: July 23rd, 2020

DOI: https://doi.org/10.21203/rs.3.rs-32494/v2

License: This work is licensed under a Creative Commons Attribution 4.0 International License. Read Full License

Version of Record: A version of this preprint was published at Nature Communications on June 3rd, 2020. See the published version at https://doi.org/10.1038/s41467-021-22713-z.

Abstract

SARS-CoV-2 enters the cell through the ACE2 receptor, which is considered one of the main inhibitors in the Renin-Angiotensin-Aldosterone System (RAAS).1 ,2 The virus has been shown to downregulate the ACE2 receptor, leading to a subsequent increase in the vasopressoragentangiotensinII.3 Evidently,criticalcoronavirusdisease2019(COVID-19)is thought to be due to a dysregulated immune response, causing a cytokine-release syndrome eventually leading to acute respiratory distress syndrome (ARDS).4 ,5 However, several reports on clinical laboratory features and case-descriptions of critically ill patients with COVID-19 show discrepancies compared to typical ARDS. Here, we show that infusing swines with angiotensin II induces a pathophysiological syndrome closely resembling that of patients with RT-PCR-positive COVID-19. By using multimodal clinical imaging of patients, comparing laboratory data and translational histological features, we show that it is highly likely that an increase in RAAS is one, if not the main, pathogenic feature in critical COVID-19. Furthermore, it is plausible that this large animal model can be used to screen for potential new treatments for patients with severe COVID-19 and that MRI lung perfusion can be used to evaluate the outcome of potential treatments targeting the pathophysiological syndrome.

Introduction

Severe acute respiratory syndrome coronavirus 1 and 2 (SARS-CoV-1) and (SARS-CoV-2) both enter human cells through cell surface angiotensin-converting enzyme 2 (ACE2) receptors.1 SARS-CoV-1 downregulates ACE2, with a subsequent increase in angiotensin II (ANGII) levels,2 which potentially creates a dysregulation with overactivation of the Renin-Angiotensin-Aldosterone System (RAAS).3 The RAAS is a hormonal system contributing to the control of circulating blood volume, blood pressure and is often pharmaceutically manipulated in hypertonic disease.4 Current clinical management guidelines for the coronavirus disease 2019 (COVID-19) are mainly centered around the assumption that SARS-CoV-2 directly results in an acute lung parenchymal disease.5,6 The possible underlying mechanisms are thought to be viral acute respiratory distress syndrome (ARDS) and/or high levels of cytokines that lead to a cytokine-release syndrome.5 However, although patients with severe COVID-19 can meet the ARDS Berlin definition, several reports in the intensive care units (ICU) at our hospital, as well as described by others, have noted relatively well-preserved lung mechanics which is not associated with a typical ARDS-pattern.6 Further, the levels of pro-inflammatory cytokines have been found to be lower than the levels expected during cytokine-release syndrome.7 Meanwhile, both preliminary reports from Wuhan and a larger retrospective cohort described that ANGII levels in COVID-19 were markedly elevated and closely associated with lung injury, while renin levels were similar to controls; strongly suggesting that plasma ANGII elevation was related to the SARS-CoV-2 infection.8,9 Furthermore, viral RNA is seldomly detected in patient plasma, one study reported viremia in only 6/41 patients and 2/15 ICU patients.10 Despite the low viral detection, currently published histopathological reports have found end organ failure in the lung, kidney, heart and small intestines, amongst others.11–16 We initiated this translational study to investigate the degree to which a disturbance in the RAAS could possibly contribute to the pathophysiological syndrome of COVID-19 and if the RAAS dysregulation could be corrected through therapeutic intervention.

Results

Retrospective imaging cohort

The clinical utility of computed tomography pulmonary artery angiography (CTPA) has been verified for monitoring of COVID-19 in our clinical setting, consistent with recent reports by other groups.17 We retrospectively analyzed all consecutive CTPA examinations acquired at Karolinska University Hospital in Huddinge, Stockholm, Sweden, in

patients with reverse transcription-polymerase chain reaction (RT-PCR) confirmed SARS-CoV-2 infection. In total, 339 CTPA examinations were performed in 289 adult patients. Motion artifacts or other technical issues prohibited pulmonary artery (PA) diameter measurements in 47 examinations, as measured by the gold standard reader, TG, resulting in 292 analyzed scans. The mean PA diameter was 29.2 ± 4.3 mm (mean ± SD), with 174 of 292 (60%) demonstrating abnormally wide PA diameter of ≥28 mm, suggestive of pulmonary hypertension.18 Pulmonary macro-thrombosis/embolism was present in 56 of 336 examinations (17%, 3 scans were not interpretable due to technical quality). We then analyzed a subset of the CTPA cohort that had also undergone echocardiography (n = 50). Echocardiography indicated high PA pressure: maximal tricuspid regurgitation velocity 3.0 ± 0.43 m/s (N=38; normal reference ≤ 2.8); estimated systolic pulmonary artery pressure 47 ± 14 mmHg (N=38; normal reference < 36); right ventricular outflow tract acceleration time 57 ± 43 ms (N=17; normal reference > 100).19,20 Maximal tricuspid regurgitation velocity and estimated systolic pulmonary artery pressure were not measurable in 12 patients due to insufficient tricuspid valve regurgitation Doppler signal.

These findings were corroborated by invasive pressure measurement obtained in a SARS-CoV-2 RT-PCR-positive 58-year-old male ICU patient. A PA-catheter was placed on ICU day 25 and recorded systolic and diastolic PA pressures of 51 ± 2.9 / 11 ± 3.2 mmHg (mean ± SD) and SvO2 of 62.4 ± 1.3 % (mean ± SD), both during the first hour after placing the catheter. Upon admission to the ICU, the patient's clinical chemistry values were PaO2 of 8.0 kPa (reference range 8.0-13 kPa) and PaCO2 of 5.1 kPa (reference range 4.6–6.0), IL-6 of 95 ng/L (reference range <7), TNF-α of 9.8 ng/L (reference range <12), C-reactive protein of 66 mg/L (reference range <3), AST of 0.53 μkat/L (reference range <0.76 D-dimer of 0.26 mg/L FEU (age-adjusted cut-off <0.58 mg/L FEU).

Clinical chemistry characteristics of imaging cohort

We retrospectively collected clinical chemistry data in the CTPA cohort based on the blood sampling closest to the exam date, within ± 3 days from the first CTPA examination. The median of D-dimer was 1.13 (lower quartile 0.66, upper quartile 3.0, reference range <0.5 mg/L FEU, n=257), fibrinogen 6.3 (lower quartile 4.6, upper quartile 7.4, reference range 2–4.2 g/L, n=91), interleukin-6 76 (lower quartile 38, upper quartile 151, reference range <7 ng/L, n=147) and TNF-α 13 (lower quartile 10, upper quartile 19, reference range <12 ng/L, n=78).

MRI lung perfusion

A clinical MRI lung perfusion scan had been performed in a SARS-CoV-2 RT-PCR-positive 61-year-old male on ICU day 22 with an initial presentation to the ICU that included a PaO2 of 7.6 kPa (reference range 8.0–13 kPa) and a PaCO2 of 3.6 kPa (reference range 4.6–6.0 kPa) by arterial blood gas; serum measurements of IL-6 154 ng/l (reference range <7 ng/L), TNF-α 10.2 ng/L (reference range <12 ng/L), C-reactive protein 242 mg/L (reference range <3 mg/L), AST 1.08 μkat/L (reference range <0.76 μkat/L) and D-dimer 0.94 mg/L FEU (age-adjusted cut-off <0.61 mg/L FEU). In this MRI lung perfusion study, the maximum contrast bolus concentration in the PA came at 15 seconds after injection and the maximum contrast bolus concentration reached the aorta after 20 seconds (Fig. 1). Using these values, we calculated a time-to-peak (TTP) map of the lungs, describing how long the injected contrast took to arrive at a specific area. The *in vivo* perfusion map presented in Fig. 1, demonstrates late contrast arrival, oftentimes later than the aortic arrival time. To further understand these paradoxical values, we measured regions of interest in the normal-appearing lungs without infiltrates, as identified by T2-weighted anatomical images.

The peripheral regions of the lungs did not receive a contrast bolus even 10 seconds after the contrast had peaked in the aorta. We manually segmented the lung and calculated the fraction of the lung with contrast peak, or no

contrast bolus at all, and found a ratio of 44% dysfunctional lung as defined by peak contrast enhancement after the aorta, suggestive of microvascular occlusion.

Summary of clinical results

We found multimodal evidence of raised pulmonary artery pressure confirmed by invasive pressure monitoring and a lack of blood perfusion in functional MRI. In a cohort of patients undergoing CTPA examination, we found no clear evidence of cytokine levels that are indicative of cytokine release syndrome, despite indication bias of sampling that would potentially skew the cohort characteristics towards those patients most ill. To further explore the implications of these findings, we turned to large animal experiments.

Large animal infusion of supraphysiological levels of angiotensin II

It seemed highly probable that at least one part of the COVID-19 pathology involved vasculature disturbances and the RAAS and we, therefore, designed a hypothesis-generating experiment where we infused ANGII in three sedated swine targeting a systolic arterial pressure of 150 mmHg. Within five minutes, arterial and PA blood pressures started to climb (Fig. S3). All three swine reached PA-systolic pressures exceeding 30 mmHg during the experiment and one swine died of acute right ventricular heart failure with extensive pulmonary thrombosis/embolism. ANGII infusion further induced a rapid decline in SvO_2, falling below 50% in all swine. Trends in arterial PaO_2 were downward and arterial $PaCO_2$ was trending upwards (Fig S4). While performing an autopsy

on Swine #1, we found a 13 cm long pulmonary thrombus. To exclude embolization, we started screening for deep venous thrombosis by ultrasonography but none were detected (Table S1). Samples for histology were acquired from macroscopically wedge-shaped blood discolored areas. After hematoxylin and eosin staining, we observed thrombotic material in small vessels, thickening of alveolar septa and debris in the alveolar sacs.

We performed bleeding time assessments in Swine #2 and #3 with baseline bleeding times of 285 seconds and 255 seconds respectively. These were reduced to < 120 seconds after 90 minutes and remained low for the remainder of the experiment. The von Willebrand factor activity (GP1bA) increased directly after the initiation of the infusion. In this hypothesis generating experiment, D-dimer increased and paradoxically, fibrinogen also increased or remained unchanged despite increased D-dimer. IL-6 and TNF-α remained below the level of detection in all swine during the experiment. Osmolality successively increased in all three swine by > 11 mosmol/kg. All clinical chemistry data is individually represented in table S1.

Infusion of supraphysiological levels of ANGII, a model akin to “accelerating the RAAS” seems to produce a remarkably unhealthy state in the swine. We hypothesize that COVID-19 patients have lost the “break” in the RAAS. Therefore, we performed additional experiments blocking ACE2 by MLN-4760.

Large animal blocking of ACE2 with low rate infusion of angiotensin II

We injected the ACE2 blocker MLN-4760 and started an infusion of ANGII in three additional swine. Increases in systemic and pulmonary artery pressures were not as high as in the supraphysiological infusion group (Fig. S3). Surface body temperature was the same, trends in PaO_2 were downward and $PaCO_2$ was trending upwards (Fig.

S4). Macroscopically, large wedge-shaped lung areas were found in the group receiving supraphysiological ANGII, highly suggestive of a more malignant model of disease by blocking ACE2. To further explore our hypothesis, we then combined the MLN-4760 blocker with the supraphysiological ANGII infusion regime. This leads to a severely malignant model with severe elevation of both systemic arterial and especially pulmonary arterial pressures, that would not be long term compatible with life (Fig. S3).

Treatment Screening in a Large Animal Model

To address the most common patient and lend mechanistic support to some of the on-going clinical trials we decided that the MLN-4760 blocker coupled with low dose infusion of ANGII might represent a clinical situation that was not as malignant as in the COVID-19 ICU patients, but could still simulate a COVID-19 patient in need of hospital intervention. Hereafter, MLN-4760 coupled with low dose infusion of ANGII will be referred to as “the animal model”. We decided to design a small study to test treatment with oral administration of 200 mg losartan, through an orogastric tube, combined with subcutaneous administration of 10,000 IU of low molecular weight heparin.

We performed MRI lung perfusion and used the same definition for peripheral perfusion deficit as in the patient, i.e. a contrast bolus peak later than the aorta or no peak at all (Fig. 1). The untreated model exhibited a significantly greater fraction of non perfused lung at 17%, compared to the treated group at 9% (n=6, SD untreated 1.5%, SD untreated 1.7%,

0.95 CI for difference 5–12, p=0.003, two-tailed t-test, assumed equal distribution). While the placebo group suffered a significant decrease in O2-saturation in the arterial blood gases over the course of the experiment (-0.54/hour), the treated group experienced no decline

(Fig. S4). The estimated difference between the groups was statistically significant (n=6, difference between groups: 0.53/hour, .95 CI: 0.096 – 0.96, p=0.017, Linear mixed error-component model, model coefficients in table S2). There were no significant differences in PaO2.

Furthermore, the PA diameter, as measured by MRI, was larger in the untreated model; 2.41 mm (SD ± 0.24) compared to 2.21 mm (SD ± 0.24) in the treated group. This difference was not significant (n=6, 0.95 CI for difference -0.3 – 0.72, p=0.32, two-tailed t-test, assumed equal distribution). These findings seem particularly interesting when considering the clinical CTPA cohort and echocardiography sub-cohorts with COVID-19, where evidence of increased pulmonary pressure, including widened PA-diameter, was observed.

During the initial hours of the animal model, no clear physiological difference could be observed between treated and untreated groups, but after approximately 2 hours systemic pressures started to return to baseline and pulmonary pressures never reached as high (Fig. S3). The estimated systolic PA pressure decreased significantly faster for the treated group compared to the untreated group which showed a trend towards higher systolic PA pressures during the intervention (n=6, -0.44/h, 0.95 CI: -0.84 – -0.040, p=0.03, linear mixed error-component model, model coefficients in table S2).

D-dimer increased in both groups, by on average 0.027 mg/L FEU per hour in placebo and 0.022 mg/L FEU per hour in the treated group. Notably, and congruent with the results from our hypothesis generating experiment, fibrinogen also increased for both groups, by 1.07 mg/L per hour in placebo and 0.47 mg/L per hour in the treated group (Table S1). Bleeding times were also reduced as in the supraphysiological ANGII infusion groups.

Echocardiography of two swine, one treated and one without treatment showed significant abnormalities in the latter, suggestive of pulmonary hypertension, with the same functional pattern as was observed in patients. The swine without treatment showed right ventricular (RV) enlargement, interventricular septal flattening, tricuspid regurgitation peak gradient > 30 mmHg, RV free wall hypokinesia and evidence of RV dysfunction.

We performed extensive histological analysis in both groups, and could confirm the same type of pulmonary damage as in the supraphysiological ANGII infused swine, predominated by a thickening of alveolar walls and debris deposition (Fig. 2). We could further discern marked end-organ damage with micro-necrotic changes in the small intestine and liver, as well as the kidney (Fig. 2).

Summary of preclinical results

We demonstrate that both “acceleration” and “loss of brake” of the RAAS, will lead to a pathophysiological phenotype closely resembling that found in COVID-19. Furthermore, we use this model to test pharmacological treatments currently under evaluation in clinical trials.

We show significant improvement in lung perfusion, as measured by MRI, O2-saturation in the arterial blood gases and PA-pressures providing mechanistic support for therapeutic strategies involving the RAAS and coagulation.

Discussion

Our results demonstrate a similar pattern between patients with COVID-19 admitted to the ICU and manipulation of the RAAS in swine. ANGII has previously been used in the ATHOSIII clinical trial.21 Sub-analyses of this trial highlighted important thrombotic and infectious complications associated with ANGII.22 If SARS-CoV-1 disturbs the distribution of the ACE2-receptor to produce a subsequent increase in ANGII,2 it is likely that the same mechanism of receptor disruption in SARS-CoV-2 leads to the effects displayed in this study. Manipulation of the RAAS in swine through both “acceleration”, by infusion of supraphysiological levels of ANGII, or “loss of brake” by ACE2 blockade and low-level infusion of ANGII, leads to a pathological phenotype closely resembling that of COVID-19. A recent study of 82 individuals with COVID-19 showed a linear relationship between ANGII levels and clinical outcome.8 The severely ill patients also had highly significant increases in ANGII as compared to controls, while renin levels remained similar, suggesting that the increase in ANGII is closely related to the SARS-CoV-2 infection. In light of that study, our large animal model blocking ACE2, coupled with a low infusion of ANGII, seems like a highly plausible model of the RAAS dysregulation in COVID-19, without directly infecting the animals with the SARS-CoV-2 virus. This model has further relevance since viremia in patients is seldom found upon testing.10 The pathophysiological syndrome of severe COVID-19 may, therefore, be explained as a downstream effect of a disruption of the RAAS, rather than blood viremia itself, given our models of both “accelerating” and “removing the brake” lead to the same panorama of end-organ damage as observed in the patients.

A hallmark of severe COVID-19 is a “ventilation pathology”. We show that this is very likely closely associated with coagulopathy in the pulmonary circulation. Using lung perfusion MRI both in a COVID-19 patient and in our swine model, without the virus, we demonstrated a reduction and in some areas likely cessation of blood flow even in absence of infiltrates. We further support these findings using CTPA and echocardiography in a retrospective patient cohort and link these with invasive pressure measurements in both patient and swine. Axial PA diameter measurements have been found to be a relatively sensitive parameter for detecting even borderline pulmonary hypertension with a sensitivity of 80% and a specificity of 62%, when using a cutoff ≥28 mm.18 In combination, our

findings provide multimodal evidence of an elevated PA resistance as a significant finding in COVID-19 patients and lung perfusion abnormalities as evaluated by MRI in both patients and swine. Furthermore, after only a matter of hours we measured upwards trending fibrinogen, despite D-dimer elevations as well as increases in blood osmolality. The same clinical chemistry findings were observed in the CTPA cohort, providing further clinical-chemistry linkage between the patients and our animal models. Our results indicate that COVID-19 patients are prothrombotic, as observed in the ICU,23 and that this may be caused by disruptions in at least two tenets of Virchow's triad, including: stasis in the pulmonary blood flow by vasoconstriction and a hypercoagulable state with increased markers of fibrin release/synthesis, plasma coagulation, von willebrand activity and bleeding time. Other publications also suggest endothelial dysfunction,11 a disruption of the third tenet of Virchow's triad. Altogether, these findings support our conclusion that severe COVID-19 is a vascular syndrome with a hypercoagulable state. If our assumptions are true, it is important to continue targeting vascular/coagulation disturbances or the dysregulated RAAS in large clinical trials. In a time of pandemic disease, we urge capable large animal laboratories to validate our findings and encourage clinical centers with MRI capabilities to evaluate the potential diagnostic power of lung perfusion MRI and its value as a readout for clinical trials. We will continue to model severe COVID-19 as a vascular syndrome to advance our understanding of the pathophysiological mechanisms driving the disease and use this model for large scale pre-clinical therapy evaluation.

References

1. Shang, *et al.* Structural basis of receptor recognition by SARS-CoV-2. *Nature* **581**, 221–224 (2020).
2. Kuba, K. *et al.* A crucial role of angiotensin converting enzyme 2 (ACE2) in SARS coronavirus–induced lung *Nature Medicine* **11**, 875–879 (2005).
3. Gheblawi, M. *et al.* Angiotensin-Converting Enzyme 2: SARS-CoV-2 Receptor and Regulator of the Renin-Angiotensin System: Celebrating the 20th Anniversary of the Discovery of ACE2. *Res.* **126**, 1456–1474 (2020).
4. Fyhrquist, & Saijonmaa, O. Renin angiotensin system revisited. *J Intern Med* **264**, 224–236 (2008).
5. Mehta, *et al.* COVID-19: consider cytokine storm syndromes and immunosuppression. *The Lancet* **395**, 1033–1034 (2020).
6. Gattinoni, *et al.* COVID-19 Does Not Lead to a "Typical" Acute Respiratory Distress Syndrome. *Am J Respir Crit Care Med* **201**, 1299–1300 (2020).
7. Qin, *et al.* Dysregulation of Immune Response in Patients With Coronavirus 2019 (COVID-19) in Wuhan, China. *Clin Infect Dis* doi:10.1093/cid/ciaa248.
8. Wu, *et al.* Elevation of plasma angiotensin II level is a potential pathogenesis for the critically ill COVID-19 patients. *Crit Care* **24**, 290 (2020).
9. Liu, N., Hong, , Chen, R.-G. & Zhu, H.-M. High rate of increased level of plasma Angiotensin II and its gender difference in COVID-19: an analysis of 55 hospitalizedpatients with COVID-19 in a single hospital, WuHan, China. medRxiv doi:10.1101/2020.04.27.20080432 (2020).
10. Huang, *et al.* Clinical features of patients infected with 2019 novel coronavirus in Wuhan, China. *The Lancet* **395**, 497–506 (2020).
11. Varga, *et al.* Endothelial cell infection and endotheliitis in COVID-19. *The Lancet* **395**, 1417–1418 (2020).
12. Fox, S. E. et al. Pulmonary and cardiac pathology in African American patients with COVID-19: an autopsy series from New Lancet Respir Med **8**, 681-686 (2020).

13. Tian, *et al.* Pathological study of the 2019 novel coronavirus disease (COVID-19) through postmortem core biopsies. *Modern Pathology* **33**, 1007–1014 (2020).
14. Ackermann, M. *et al.* Pulmonary Vascular Endothelialitis, Thrombosis, and Angiogenesis in Covid-19. *New England Journal of Medicine* **382**, 1653-1659 (2020).
15. Su, *et al.* Renal histopathological analysis of 26 postmortem findings of patients with COVID-19 in China. *Kidney International* **98**, 219–227 (2020).
16. Ignat, *et al.* Small bowel ischemia and SARS-CoV-2 infection: an underdiagnosed distinct clinical entity. *Surgery* **168**, 14–16 (2020).
17. Poissy Julien *et* Pulmonary Embolism in COVID-19 Patients: Awareness of an Increased Prevalence. *Circulation* **0**,.
18. Mahammedi, A., Oshmyansky, A., Hassoun, M., Thiemann, D. R. & Siegelman, S. S. Pulmonary artery measurements in pulmonary hypertension: the role of computed tomography. *J Thorac Imaging* **28**, 96–103 (2013).
19. Yared, *et al.* Pulmonary artery acceleration time provides an accurate estimate of systolic pulmonary arterial pressure during transthoracic echocardiography. *J Am Soc Echocardiogr* **24**, 687–692 (2011).
20. Milan, A., Magnino, C. & Veglio, Echocardiographic indexes for the non-invasive evaluation of pulmonary hemodynamics. *J Am Soc Echocardiogr* **23**, 225–239; quiz332–334 (2010).
21. Khanna, A. *et al.* Angiotensin II for the Treatment of Vasodilatory *New England Journal of Medicine* **377**, 419–430 (2017).
22. Farina, N., Bixby, & Alaniz, C. Angiotensin II Brings More Questions Than Answers. *P T* **43**, 685–687 (2018).
23. Klok, A. *et al.* Incidence of thrombotic complications in critically ill ICU patients with COVID-19. *Thromb. Res.* **191**, 145–147 (2020).
24. Lange, J. *et al.* Increased pulmonary artery diameter on chest computed tomography can predict borderline pulmonary hypertension. *Pulm Circ* **3**, 363–368 (2013).

Declarations

Acknowledgements

We would like to thank Pellina Jansson, Johanna Doshé, Britt Meijer, Ann-Christine Sandberg-Nordqvist, Anette Ebberyd, Niklas Bark and Lisbeth Söderblom for excellent logistic and technical assistance. Furthermore, we would like to acknowledge the helpful assistance regarding MRI by Magnus Tengvar and Thelma Gudmundsdóttir at the Department of Radiology Solna, Karolinska University Hospital. We would also like to acknowledge colleagues from the Department of Neuroradiology, Karolinska University Hospital, for critical discussion regarding perfusion imaging. Finally, we would like to thank Stina Englesson for assistance with graphical illustrations.

Competing interest

The authors declare no competing interests. TG was supported by grants from the Stockholm Region ALF and Clinical Postdoc programs. JL was supported by grants from the Stockholm Region Clinical Postdoc program, a private donation by Tedde Jeansson Sr andMedTechLabs at Karolinska Institutet. JL holds stock options in SmartCella Holding AB and owns LRLJ2R Consulting AB. Both companies are unrelated to this work.

Author contributions

SR and JL initiated the study. JA, MK, RO, TG and JL analyzed computed tomography pulmonary angiography data. GA analyzed both clinical and preclinical echocardiography data. SR and FCJ performed the clinical pulmonary artery catheter measurements and analyzed the data. SR and FCJ stressed the need for adequate imaging in COVID-19 and took care of the ICU patient during the clinical MRI. RVP and JL optimized the clinical MRI protocol. SN and JL interpreted the clinical MRI study. SR, MJF and JL designed the animal studies and together with JA performed the animal studies and analyzed data. RO, MP, TG and JL optimized the preclinical MRI protocol. RO, MP and TG performed the preclinical MRI scans and TG; JL analyzed the data. JA, RO, TG and JL performed pre-clinical histological evaluation. AS identified the need for interleukin analyses and analyzed the data. SR, AS, MF, MJF and JL analyzed clinical chemistry data. HE, RO, TG and JL performed statistical analysis. TG, MJF and JL supervised the study. JL wrote the first draft and all authors revised the manuscript critically.

Data and materials availability

All data is available in the manuscript or the supplementary materials. The authors will freely make available any materials and information associated with their publication that are reasonably requested by others for the purpose of academic, non-commercial research.

Figures

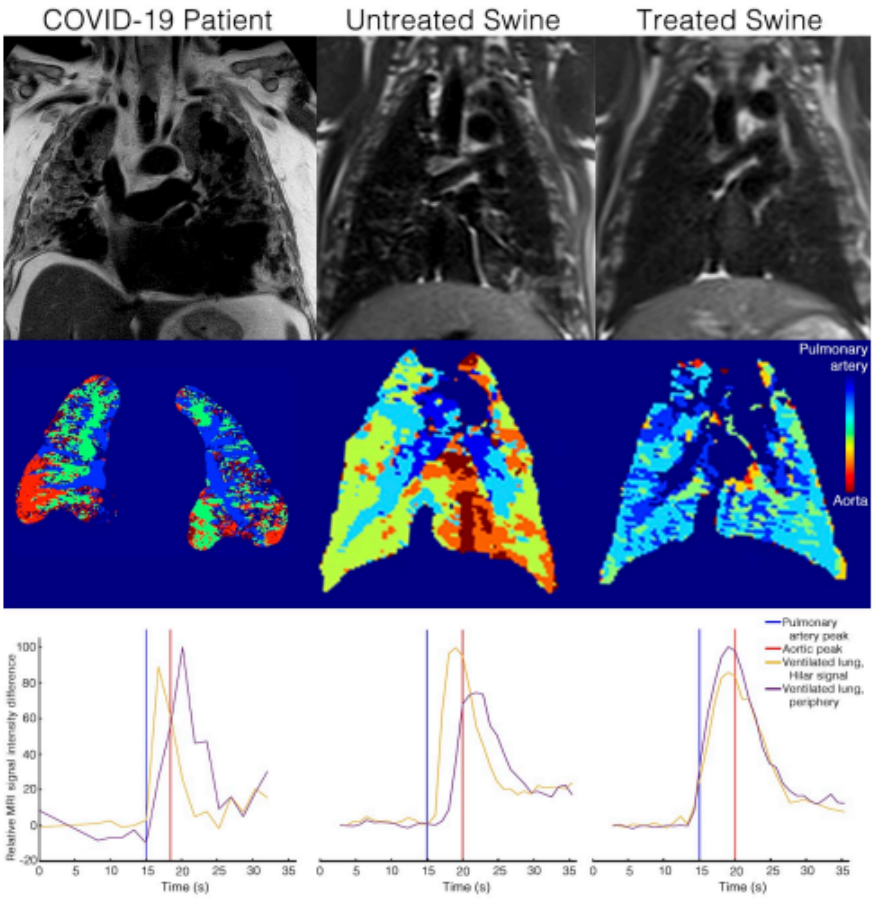

Figure 1

MRI of a patient with COVID-19 and swine with/without treatment showing severe peripheral perfusion deficits. The first column represents the patient with lung perfusion MRI, while the second represents a swine treated with MLN-4760, an ACE2 blocker, and low dose ANGII infusion followed by a swine given MLN-4760, ANGII and treatment with losartan and low molecular weight heparin. Top row: Anatomical coronal T2-weighted imaging used to ensure that the regions of interest were placed in lung tissue with a normal-appearing T2 signal. Middle row: Coronal time-to-peak (TTP) maps where the color lookup table is set so that blue corresponds to the contrast TTP in the pulmonary artery and yellow the TTP in the aorta. Bottom row: Time Intensity curves in a region of interest in a hilar (yellow) and peripheral (purple) region without infiltrates. The blue and red vertical lines represent the pulmonary artery and aortic peaks respectively. The TTP is delayed (even after the aortic peak) in both the patient and the untreated animal model, suggestive of hypoperfusion. Meanwhile, in the animal model treated with losartan and low-molecular-weight heparin, both the hilar and peripheral peaks occur before the aortic peak, as expected in normal physiology.

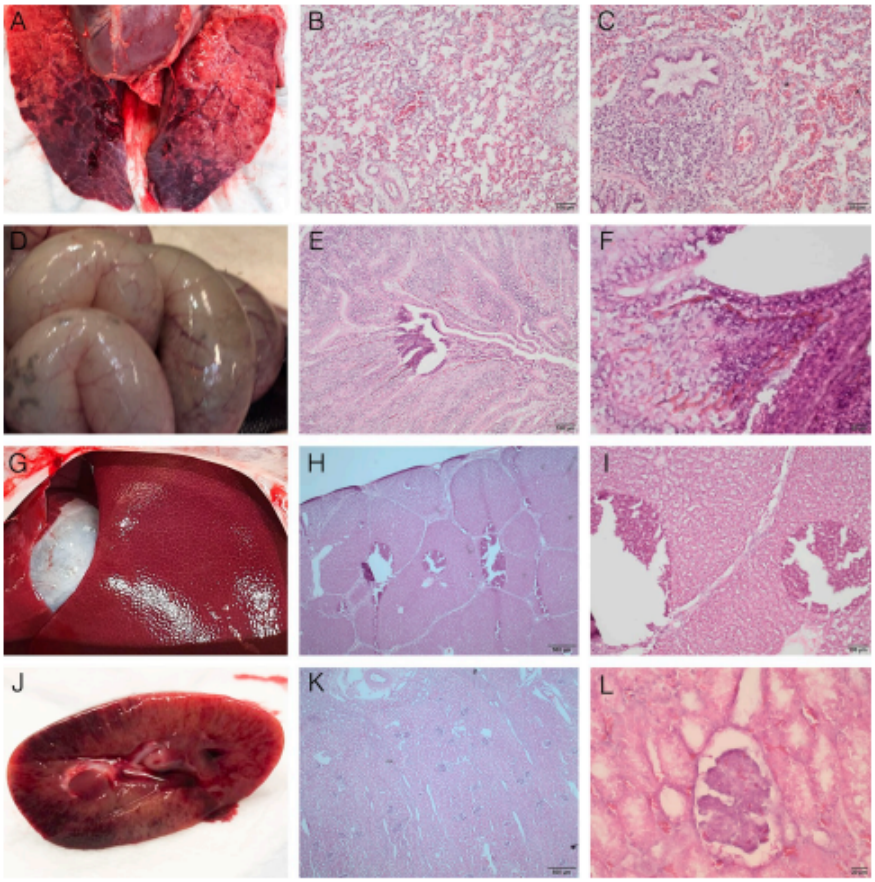

Figure 2

Macroscopic and microscopic findings in untreated swine with the ACE2 blocker MLN-4760 and low-dose angiotensin II infusion. Lung with macroscopic infarcts (A). Thickened alveolar walls, occlusion of vessels and debris in micro bronchi in low (B) and high (C), magnification. Small intestine, gas-filled and partially distended (D), with microscopically dark stained necrosis in the most distal microvilli in low (E) and high magnification (F), including heavy inflammatory infiltration. Liver, macroscopically normal (G), with necrotic dark stained areas in the periphery and around the central venule at low magnification (H), and high magnification (I). Kidney with macroscopically multiple dark stained necrotic areas (J). Low magnification (K), and high magnification (L) showing a necrotic bowman capsule.

Supplementary Files

This is a list of supplementary files associated with this preprint. Click to download.

- supplement1.pdf
- Methodsethicsstatementsupplementalfiguresandtables.pdf
- supplement2.pdf
- ChangelogCoronavirusdisease2019maybedrivenbyanoveractivationofthereninangiotensinaldosteronesystem.pdf